High-Power Solar Inverter Efficiency Measurements by Calorimetric and Electric Methods

Lassi Aarniovuori, Antti Kosonen, Pekka Sillanpää, and Markku Niemelä

***Abstract*—In this paper, the results of a European efficiency measurement for a 250-kW high-efficiency grid-connected solar inverter are presented. The efficiency measurements are performed both by electrical input–output and calorimetric methods. Two measurement series with input voltage levels of 500 and 750 VDC are carried out. An open- and balance-type calorimeter system that can measure power losses up to 30 kW is introduced and verified by resistor tests. The measurement results and their uncertainty are analyzed and discussed.**

***Index Terms*—Calorimetry, converters, efficiency, measurement, photovoltaic (PV).**

I. Introduction

WHILE the photovoltaic (PV) effect has been known for more than 150 years, and the solar cell technology has already reached its 50-year milestone, a comprehensive approach to the solar energy supply (including the power electronic converters) has only recently raised the interest of the markets. Over the past decade, there has been a growing demand for renewable resources, especially in the area of solar energy. The rapid growth is mainly due to the national programs of feed-in tariffs in many countries, which have established a competitive price for the renewable energy producers. With the increasing demand, the total efficiency has become a highly important issue.

Solar inverters play an important role in the cost effectiveness for energy producers, and companies in the market make use of the efficiency-oriented approach in their sales arguments. Since the mid-1990s, the solar inverter efficiency has improved from around 90% up to 99% as a whole [1], [2]. New approaches, such as modular grid-connected PV systems [3], [4], new maximum power point tracking (MPPT) algorithms and realizations [5]–[7], multilevel topologies [8]–[12], soft switching [13], output filter optimization [14], and silicon carbide semiconductors [15], have been adopted to further raise the efficiency level. The efficiency of a solar inverter is based on the conversion efficiency, as presented in [16], and the (MPPT) efficiency. In [17], a quantity of "total efficiency" is introduced to characterize the solar inverter performance. Traditionally, the performance of a solar inverter has been measured in terms of weighted factors, such as the European and Californian efficiency [18].

The efficiency measurement in switched-mode power electronic devices is not a straightforward task. As a result of the pulsewidth modulation (PWM) behavior of the inverters, challenges arise from the wide frequency spectrum of the current and voltage. Furthermore, the applied instrumentation settings may cause significant variation in the results, as shown in [19]. So far, the measurement uncertainty related especially to high-power and high-efficiency devices has received little attention in the study of power electronics, and the calorimetric measurement method is not usually used despite the fact that the calorimetric method is the preferred method to determine the total losses of large generators and motors [20]. With high-efficiency devices, the application of the conventional electrical input–output method becomes even more challenging because of the uncertainty of the loss measurements. An alternative to the electrical loss measurement is provided by the calorimetric method. By a calorimeter, the losses are measured directly from the generated heat, and the measurement uncertainty is independent of the efficiency. Moreover, the calorimetric measurement method is independent of voltage and current waveforms and their phase shift. The calorimetric method allows the measurement of the converter efficiency with any modulation method or switching frequency with a comparable accuracy. By the equation

$$\eta = \frac{P_{\mathrm{out}}}{P_{\mathrm{in}}} = \frac{P_{\mathrm{in}} - P_{\mathrm{tl}}}{P_{\mathrm{in}}} = \frac{P_{\mathrm{out}}}{P_{\mathrm{out}} + P_{\mathrm{tl}}} \tag{1}$$

where η is the overall efficiency (%), P_{in} the input power to the component (W), P_{out} the output power from the component (W), and P_{tl} the total power loss (W); the measured losses are converted into efficiency. With the calorimeter, a characteristic of particular interest is that as the efficiency approaches 100%, the uncertainty of the efficiency approaches zero. The phenomenon is illustrated and compared with the characteristics of the input–output method in Fig. 1.

In this paper, a European efficiency measurement for a 250-kW grid-connected solar inverter is performed both by electrical input–output and calorimetric methods. The solar inverter is a modified prototype for the university use. It is of a standard two-level construction with a three-phase full bridge and an output filter. Two measurement series with input voltage levels of 500 and 750 VDC are conducted. To the best of the authors'

Manuscript received June 1, 2012; revised August 3, 2012 and September 12, 2012; accepted September 13, 2012. Date of current version December 7, 2012. Recommended for publication by Associate Editor T. Suntio. This work was supported in part by the European Regional Development Fund, the City of Lappeenranta, ABB Oy, Vacon PLC, The Switch, and LUT Energy, Lappeenranta University of Technology.

L. Aarniovuori, A. Kosonen, and M. Niemelä are with the Department of Electrical Engineering, Institute of Energy Technology, Lappeenranta University of Technology, FI-53851 Lappeenranta, Finland (e-mail: lassi.aarniovuori@lut.fi; antti.kosonen@lut.fi; markku.niemela@lut.fi).

P. Sillanpää is with the Department of Electrical Energy Engineering, Tampere University of Technology, FI-33720 Tampere, Finland (e-mail: pekka.e.sillanpaa@tut.fi).

Color versions of one or more of the figures in this paper are available online at http://ieeexplore.ieee.org.

Digital Object Identifier 10.1109/TPEL.2012.2221166

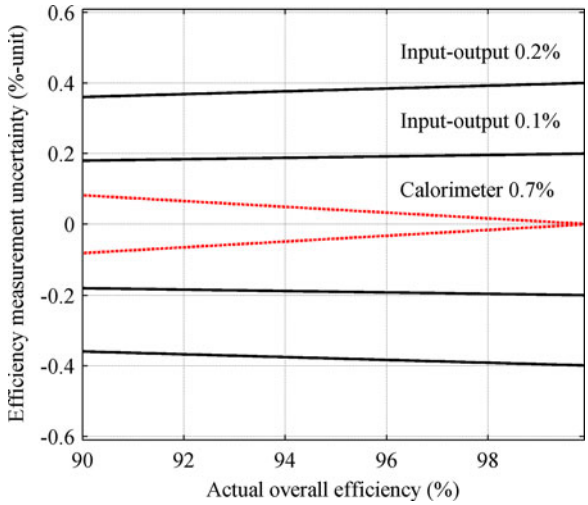

Fig. 1. Measurement uncertainty of efficiency in percent units with the input–output method as a function of actual overall efficiency with an electric power measurement uncertainty of either 0.1% or 0.2% (continuous line). The uncertainty is the same both for the input and output powers. This figure also illustrates a similar case where the power losses are measured by a calorimeter with a measurement uncertainty of 0.7%, and the input power is measured with a 0.2% uncertainty (dashed line). The uncertainty is at maximum with the electrical method and at minimum with the calorimeter in the 100% efficiency point.

knowledge, this is the first time that the calorimetric measurement results of a high-power solar inverter are presented.

This paper is organized as follows. Section II concentrates on the proposed calorimetric system. Section III presents the equations for the calorimetric loss calculation. Section IV discusses the laboratory measurements with the high-power solar inverter prototype. The measurement uncertainties of the applied methods are analyzed in Section V. Section VI discusses the results, and Section VII concludes the paper.

II. Calorimetric System Applied in the Measurements

A review of previously reported calorimetric systems is presented in [21]. These calorimeters can be divided into two basic types: an open type with air as a coolant and a closed type with water as a coolant. The open- and balance-type calorimeters are introduced in [22]–[25]. In addition, there are calorimetric systems called direct calorimeters in which the balance test is replaced by measurements [26]–[29].

The designed system is an open- and balance-type calorimeter. The open-type system makes it possible to use the necessary additional cablings (other than power) for the device under test (DUT). The basic idea of a balance-type calorimeter is to define the heat losses of a device with the balance test of a reference heater. The balance test is carried out at night time, and hence, the measurement rate of a single test point per day is maintained. The variation in the air properties over the test period and different temperature gradients through the chamber walls between two tests are taken into account by the temperature T, humidity φ, and barometric pressure p measurements.

The calorimeter is designed to measure heat losses between 2 and 30 kW. The system is illustrated in Fig. 2. The internal

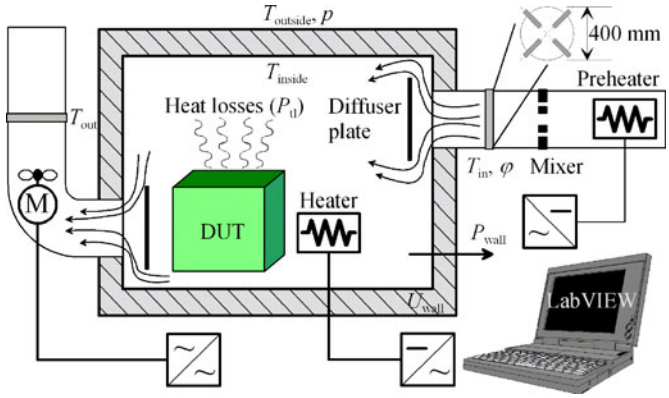

Fig. 2. Concept of heat loss measurements.

dimensions of the chamber are 2.0 m × 2.0 m × 2.5 m ($l \times w \times h$). A smaller version with the same operating principles has been used to determine inverter losses [30] and induction motor losses under sinusoidal and PWM supplies in [31]. The basic construction is a sealed box insulated with a 100-mm polyurethane plane. The operating temperature is controlled by the blower speed in the full heat loss range. The operating temperature is kept 15 K higher than the temperature of the surrounding air, but the temperature can also be varied. The blower is driven by a vector-controlled frequency converter with a speed feedback. The blower is located at the bottom of the chamber as illustrated in Fig. 2. The inlet tube is located at the top of the chamber. The maximum volume flow of the blower is scaled to 4500 m^3/h for blower dimensioning purposes to remove 30-kW heat losses. For this task, a radial blower is selected. The blower is a three-phase 2.7 kW one with a nominal rotation speed of 830 r/min.

For the balance test, a basic steel-grid-fixed resistor is applied as a heater that withstands 30 kW of continuous dc power. The heater is also applied when the chamber is heated before the measurements. This way, the thermal equilibrium state can be reached faster. The resistor is driven by a dc power supply. The dc power is measured by a power analyzer with a power accuracy of 0.1% of the reading + 0.1% of the range. The preheater driven by a dc power supply is used to keep the inlet air at a constant temperature. A PI controller with the inlet air temperature feedback is controlling the preheater power.

A-class PT-100 temperature sensors with four-wire compensation circuits are applied to measure the temperatures. The temperature sensors are read by a data acquisition system with a 40-channel differential multiplexer module. The system resolution is 0.01 K, and the accuracy is ±0.06 K plus the sensor error $\pm(0.15 + 0.002|T|)$ K. The measuring uncertainty of humidity is ±2% RH within 0–90% RH range, and the barometric pressure uncertainty is ±70 Pa. The inlet and outlet temperatures ($T_{\rm in}$ and $T_{\rm out}$) are averaged from four sensors (see Fig. 2). The inlet and outlet tubes have a mixer (blower in the outlet) to equalize the temperature inside the tube before the temperature sensors. The inside temperature distribution of the chamber $T_{\rm inside}$ is measured from a grid of 16 sensors and the outside temperature distribution of the chamber $T_{\rm outside}$ from four sensors (in the

Fig. 3. Experimental setup of the calorimeter. The insulated chamber with a heater and a solar inverter inside.

center of each wall). There are diffuser plates in the front of the inlet and outlet tubes to remove direct heat radiation to the tubes. This removes the effect of the locations of the heat sources in the chamber on that proportion of the heat power that is transferred by the air flow. Therefore, the location of the heat source is only affecting that proportion of the losses that are a result of the heat leakage through the walls. All the measurements, controls, algorithms, and data processing are implemented to a control computer via a LabVIEW interface. Fig. 3 illustrates the experimental setup of the calorimeter.

III. Measurement Procedure for Heat Losses

The measurement procedure consists of two parts: the main and balance tests. The idea in the main test is to heat the chamber with the DUT as long as the system is in the thermal equilibrium state at the desired operating temperature. The main test is started with the preheated chamber by driving the DUT in a desired operating point. The PI controller is used to keep the outlet temperature at about 40 °C by controlling the blower rotation speed. The rotation speed is set to a fixed value after the system has reached close to the thermal equilibrium state. The fixed speed value is kept to reach the final thermal equilibrium state. After the thermal equilibrium has been achieved (the power estimate does not change) in the main test, the DUT is switched OFF, and the rotation speed of the blower is still kept fixed. If the DUT contains a blower, it is also kept on in the balance test to keep the ventilation constant. The estimated total power loss of the DUT in the main test is supplied to the heater. The estimate is received from the calibration test, where the heating power is calibrated with the rotation speed. The time to reach the thermal equilibrium state depends on the mass inside the chamber and how close to each other the estimated and actual heat losses are. The balance test is driven so long that the thermal equilibrium state is reached with the heater.

After the blower speed has been fixed, also the mass flow rate is fixed when the average specific heat capacity through the chamber is used. The total heat losses of the DUT in the thermal

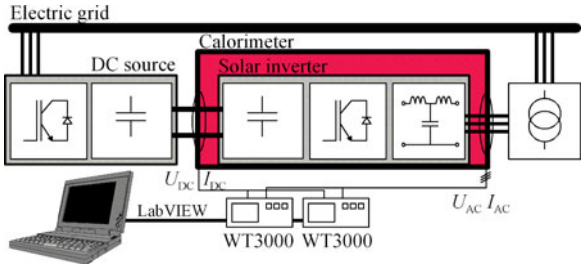

Fig. 4. Laboratory equipment for the efficiency measurement.

equilibrium of the calorimeter can be expressed as

$$P_{\mathrm{tl}} = \bar{c}_{\mathrm{p}} q_{\mathrm{m}} \Delta T_{\mathrm{air}} + U_{\mathrm{wall}} S_{\mathrm{wall}} \Delta T_{\mathrm{wall}} \tag{2}$$

where $\bar{c}_p$ is the specific heat capacity of the moist air (J/kg·K) calculated with the average temperatures of the inlet and outlet air, q_m the mass flow rate (kg/s), ΔT_{air} the temperature difference of the moist air between the inlet and outlet tubes (K), U_{wall} the overall heat transfer coefficient of the chamber (W/m^2·K), S_{wall} the area of the chamber walls (m^2), and ΔT_{wall} the temperature gradient across the chamber walls (K). ΔT_{wall} is calculated based on the inside temperature T_{inside} and the outside temperature T_{outside}. In (2), only the mass flow rate is an unknown variable. The estimated mass flow rate $\hat{q}_m$ can be computed based on (2) and the known heater power P_{tl} during the balance test as follows:

$$\hat{q}_m = \frac{P_{\mathrm{tl}} - U_{\mathrm{wall}} S_{\mathrm{wall}} \Delta T_{\mathrm{wall}}}{\bar{c}_p \Delta T_{\mathrm{air}}}. \tag{3}$$

The total power losses in the main test are computed by (2) with the estimated mass flow rate combining the calculated heat losses through the walls in the main test. The differences in the measured variables $(T_{\mathrm{in}}, T_{\mathrm{out}}, T_{\mathrm{inside}}, T_{\mathrm{outside}}, p, \varphi)$ between the main and balance tests are taken into account when the losses are calculated. A typical heat leakage through the chamber walls with a 15 K temperature difference is about 200 W. By calculating (3) during the main and the balance test, it is possible to determine when the thermal equilibrium has been reached. Hence, as the exact value of the mass flow rate is not known during the main test, a constant value or an interpolated value of the previous calibration measurements is used.

It should be noted that the estimated mass flow rate includes all the errors made in the measurements, because they are calibrated with the heater used in the balance test. The heat losses in the main test are fitted according to the balance test by applying the air properties to the data processing. The accuracy of the calorimetric measurement results is degraded if the system is not in a thermal equilibrium state in both tests.

IV. Laboratory Measurement

The measurement setup is illustrated in Fig. 4. The line converter was used as a dc input source of the solar inverter to emulate the operation of the PV cells. The DUT includes a prototype solar inverter with an output filter. The solar inverter ac output was connected to the grid through a transformer. The solar inverter was measured in the power reference mode, because

TABLE I
NUMERICAL RESULTS OF THE EFFICIENCY MEASUREMENTS

		500 VDC						750 VDC					
	Power ref.	100%	50%	30%	20%	10%	5%	100%	50%	30%	20%	10%	5%
Current shunt	U_{in1} (V)	496.7	500.1	502.3	501.6	505.9	507.4	750.1	751.0	751.0	751.2	751.4	751.6
	I_{in1} (A)	514.2	255.6	153.5	103.7	53.7	30.1	339.8	171.1	105.5	72.9	40.4	24.4
	P_{in1} (W)	253078	126764	76330	51192	25996	13278	253571	126899	76857	51857	26709	14371
	U_{out1} (V)	311.6	310.9	309.8	307.9	308.8	308.2	311.2	308.3	309.6	307.9	314.0	310.4
	I_{out1} (A)	462.2	234.3	143.0	97.6	52.7	34.0	461.7	237.2	147.1	103.1	62.9	47.7
	P_{out1} (W)	248410	124891	75096	50189	25208	12544	247312	124185	74639	50142	25132	12548
Zero-Flux™	U_{in2} (V)	496.6	499.9	502.1	501.5	505.7	502.4	750.0	750.8	751.0	751.1	751.3	751.3
	I_{in2} (A)	514.5	255.0	152.5	102.4	51.8	27.6	338.6	169.4	102.3	69.2	35.9	19.3
	P_{in2} (W)	253369	126789	76169	51014	25831	13268	253427	126918	76579	51753	26591	13838
	U_{out2} (V)	311.5	310.9	309.8	307.9	308.7	306.3	311.2	308.3	309.6	307.8	312.4	310.3
	I_{out2} (A)	461.6	233.6	142.1	96.7	51.6	32.5	459.3	233.4	140.9	96.4	51.9	32.0
	P_{out2}(W)	248104	124705	74957	50097	25184	12543	247031	123991	74501	50035	25114	12559

the dynamic power variation in the MPPT is not suitable for the calorimetric measurement. Therefore, the conversion efficiency was measured in each operation point, in which the solar inverter was driven from 4 to 8 hours. Electric and calorimetric measurements are performed in the same measurement cycle. Thus, the surrounding temperature of the DUT is the same in both measurements. The solar inverter efficiency was measured with 500 and 750-VDC input voltage levels, and the loads were chosen to be 5%, 10%, 20%, 30%, 50%, and 100% of the nominal load as specified for the EU efficiency in the standard EN 50530.

Two four-module Yokogawa WT3000 power analyzers were used to perform the electrical measurements during the calorimetric measurement. The first WT3000 was equipped with HILO WSM600 current shunts (600-A RMS maximum current) and the second one with a HITEC Zero-Flux current (3000-A maximum peak current) measurement system. Both power analyzers measured the input RMS current $I_{\rm in}$, the input voltage $U_{\rm in}$, the input power $P_{\rm in}$, the output RMS current $I_{\rm out}$, the output voltage $U_{\rm out}$, and the output power $P_{\rm out}$. The numerical values are gathered in Table I.

In the nominal point, the input and output current values of the two separate analyzers have a difference of 0.28 and 0.63 A, respectively. The current difference increases when the power is decreased. The maximum difference in the dc input voltage is 4.9 V and in the input current 2.5 A in the operating point with a 5% power reference. An ac output voltage difference of 1.9 V and an ac current difference of 1.6 A are detected in the same operating point. The first power analyzer measures a 292-W (-0.12%) lower input power and a 305-W ($+$ 0.12%) higher output power in the nominal point than the second power analyzer.

In the measurement series with 750 VDC, the first power analyzer gives a 1.2 A higher input and a 1.3-A output current value than the second one in the nominal point. Similarly as with the 500-VDC series, the difference increases when the power reference is decreased. With the 5% power reference, the difference is 5.2 A in the input and 15.7 A in the output current. Thus, this leads to an input power difference of 533 W (4.2%). This power difference is quite high when compared with the total losses in this load point.

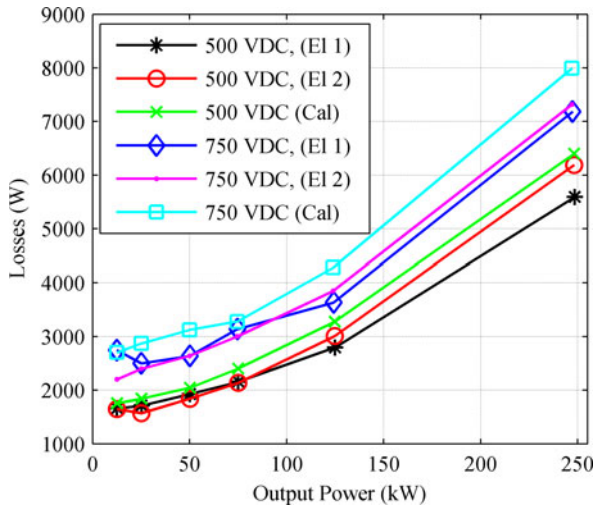

Fig. 5. Solar inverter losses as a function of output power.

The solar inverter losses consist mainly of semiconductor switching and conduction losses, and of output filter iron and copper losses. Other minor sources of losses are, for example, the dc link and the electromagnetic interference filters. In addition, there are inverter-related losses caused by auxiliary devices. These losses are produced for instance by the microcontroller, internal power supply, display, keyboard, bus communication, digital and analogue inputs and outputs, and exhaust blowers. The majority of this power consumption is due to a three-phase blower that ventilates the output filter cabinet. This auxiliary device loss is added to the electrical measurements, because the calorimeter measures the total heat losses. The power loss results and the efficiencies are shown in Figs. 5 and 6.

The results in Figs. 5 and 6 show that the inverter efficiency decreases when the dc input voltage is increased. The losses measured with the calorimeter are slightly higher in all measurement points. With the nominal power reference of 250 kW, the loss difference between the calorimetric and electrical measurement is 700 W with 750 VDC. The results measured with a power analyzer equipped with Zero-Flux sensors are close to

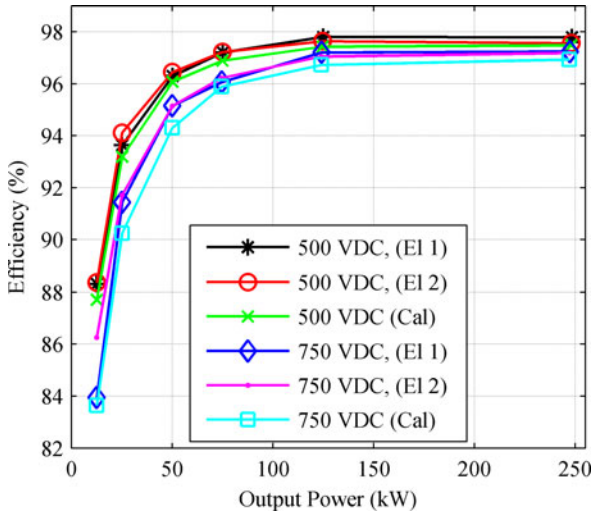

Fig. 6. Solar inverter efficiencies as a function of output power. The calorimetric efficiencies are calculated using the electric output power.

TABLE II
RESULTS OF THE HEATER TEST

Measured DC power, main test (W)	Calorimetric result (W)	Uncertainty (W)	Uncertainty (%)
2000.00	2007.97	+7.97	+0.29
3000.00	2982.69	–17.31	–0.46
4000.00	3977.96	–22.04	–0.47
5000.00	4994.93	–5.07	–0.09
6000.00	6034.17	+34.17	+0.51
7000.00	7020.87	+20.87	+0.27

those of the calorimeter, whereas the other Yokogawa power analyzer with current shunts yields 600-W lower losses.

V. MEASUREMENT UNCERTAINTY

A. Calorimeter

Six different reference power levels between 2 and 7 kW, covering the range of the solar inverter heat losses, were used to validate the calorimeter performance. The balance test heater was used to emulate the measured heat source. The power to the heater is provided by a programmable dc power supply using the actual power recorded from the terminals of the resistors inside the calorimeter by a digital power analyzer. The measurement procedure is exactly the same as when measuring the solar inverter. The solar inverter is inside the chamber during this verification test. The cooling blower of the solar inverter and the heater was used in the tests.

The verification results are given in Table II. The powers are scaled to the same level, and the type A evaluation of uncertainty is applied to these six measurement points by using Student's t-distribution. The uncertainty of the calorimeter is 0.41% and for the power analyzer 0.58%. According to [32] and the results, the combined (calorimeter and dc power measurement) standard uncertainty for the calorimeter is about ±0.7% with a confidence level of 95% for powers between 2 and 7 kW.

The basic principle of a calorimetric device is to directly measure the total power losses P_{tl}. Together with the input power P_{in} measurement, it can be considered to be the most accurate method to define efficiency. In this case, it is obvious to use the output power measurement instead of the input power, because the power analyzer measures ac power more accurately than dc power.

TABLE III
MEASUREMENT EQUIPMENT UNCERTAINTIES

Device	DC uncertainty	AC uncertainty
WT3000	±(0.05% + 0.05%)	±(0.01% + 0.03%)
CURACC	±(0.002% + 0.001%)	±(0.01% + 0.002%)
HILO	calibrated ±0.02%	calibrated ±0.02%

B. Electrical Measurement

Digital power analyzers are used to perform power measurements. This kind of a digital meter takes simultaneous samples of currents and voltages, digitizes these values, and provides arithmetic multiplication and averaging by applying digital techniques to obtain the power measurement [33].

The power analyzer accuracy is given as a sum of the reading uncertainty and the measurement range uncertainty. The uncertainties considering the electrical equipment used in the measurements are shown in Table III.

The power measurement uncertainty of the power analyzers is given for sinusoidal signals with a unity power factor in the given frequency range. Additional uncertainties arise from the leading or lagging power factors and common-mode voltages in the measurement system, and the distortion of the voltage and current signals. A typical direct input range of the digital power analyzers is up to 50 A, and therefore, the currents of power converters and motor drives are measured by current transducers that add their own uncertainty to the measurement system. Therefore, it is a complex task to define exact uncertainty bounds for the power measurement of PWM signals that hold multiple frequencies. The current shunt outputs a 60-mV signal with a nominal 600-A load (RMS), and Zero-Flux outputs a 1-A signal with a nominal 3000-A load (peak).

C. Comparison of Uncertainties Between the Input–Output and Calorimetric Methods

The type B standard uncertainty analysis is carried out for the input–output measurements. The input estimate values x_i of the quantity X_i make up an output estimate according to the function $y = f(x_1, x_2, \ldots, x_N)$. The input quantities are considered not to correlate. The combined standard uncertainties of efficiency measurements are calculated according to [32] by means of an uncertainty budget

$$u_c(y) = \sqrt{\sum_{i}^{N} \left(\frac{\partial f}{\partial x_i}\right)^2 u^2(x_i)}. \tag{4}$$

The ac power uncertainty is multiplied by the factor of $\sqrt{2}$ to include the effect of the two-wattmeter method in the uncertainty contribution. In the laboratory setup, the important factors contributing to the uncertainties are the power analyzer range

TABLE IV
WT3000 RANGE SETTINGS

Range	Shunts	Zero-Flux
UDC	1000 V	1000 V
UAC	600 V	600 V
IDC	0.1 V	0.5 A
IAC	0.1 V	0.5 A

settings for the current and the voltage values. The values are shown in Table IV.

The combined uncertainty for the efficiency in a measurement point can be determined based on the uncertainties of the measured dc and ac power. The uncertainty quantities are decided based on the laboratory setup consisting of the power analyzer and current measurement device uncertainty factors. The estimate of the input quantity is multiplied by the uncertainty of the particular measurement instrument to obtain the standard uncertainty. A sensitivity coefficient $c_i = \partial f / \partial x_i$ is needed to achieve the contribution of the aforesaid to the combined standard uncertainty $u_i(y) = c_i u(x_i)$. Finally, the combined standard uncertainty $u_c(y)$ of the measurement result is obtained as a root sum square of the uncertainty contributors.

Let us consider an uncertainty contribution calculation for the dc current shunt for the values with the 100% power reference given in the first column of Table I. The input estimate for the resistance is 100 $\mu\Omega$. The uncertainty of 0.02% is considered normal distributed by the confidence level of 95%, by which we obtain a coverage factor of 2 to transform the uncertainty to the one sigma level. The standard uncertainty $u(x_{\text{shunt}})$ is thus

$$u(x_{\text{shunt}}) = \frac{100\,\mu\Omega \times 0.02\%}{2} = 10\,\text{n}\Omega. \tag{5}$$

The sensitivity coefficient is calculated as

$$c_{\text{shunt}} = \frac{\partial P}{\partial R} = \frac{P_{\text{DC}}}{R_{\text{shunt}}} = \frac{253078\,W}{100\,\mu\Omega} = \frac{2.53\,\text{W}}{\text{n}\Omega}. \tag{6}$$

Thus, the uncertainty contribution to the shunt yields

$$u_{\text{shunt}}(y) = c_{\text{shunt}}\, u(x_{\text{shunt}}) = 25.3\,\text{W}. \tag{7}$$

The calculated measurement uncertainty limits are shown in Fig. 7. The uncertainty limits are narrow when the nominal power is used, and they become broader when the power is reduced. The Yokogawa power analyzer equipped with Zero-Flux sensors has the worst uncertainty ranges, which is a result of the nominal value of the current sensors. The uncertainty ranges in each measurement point fit each other.

The measurement equipment for the electrical input–output method determines the uncertainty components for the input and output powers. As it can be seen in Fig. 8, there is a certain dominating component in the uncertainty budget that imposes a limit on the combined uncertainty minimum level. The dominating component should be reduced in order to decrease the total uncertainty because of the root-sum-square nature associated with the behavior of the combined uncertainty. For example, the WT3000 range and the reading uncertainties of 0.05% with dc are the dominating components compared with the current-shunt-calibrated accuracy of 0.02% and the Zero-Flux accuracy

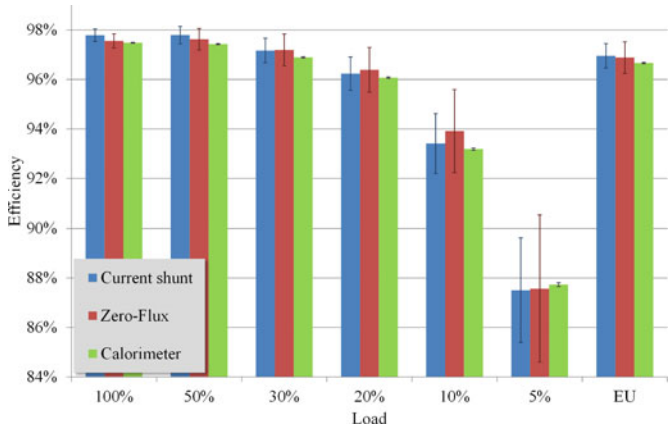

Fig. 7. Expanded uncertainty limits of the efficiency measurements at 500 VDC. With the highest load values, the calorimetric method uncertainty in the efficiency is difficult to distinguish.

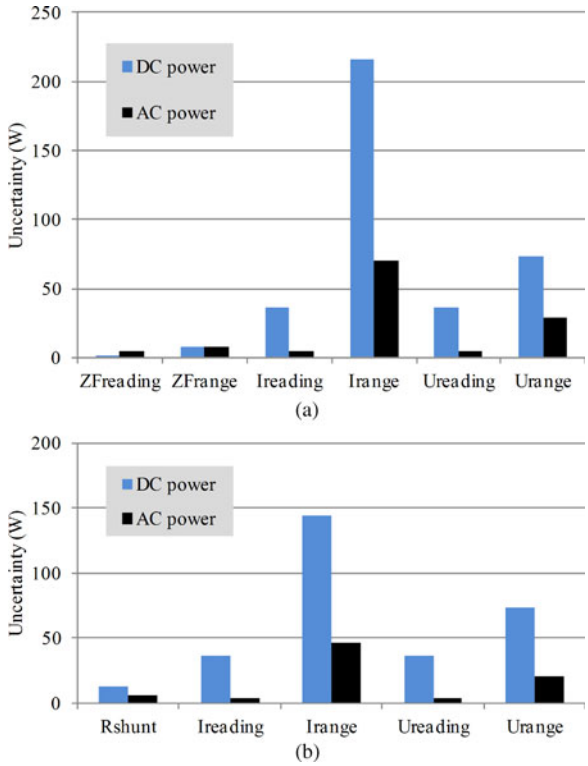

Fig. 8. Uncertainty distribution at a 50% load based on the power analyzer and current transducer uncertainties in (a) Zero-Flux- and (b) current-shunt-based efficiency measurements.

of $\pm(0.002\% + 0.001\%)$ if optimal signal ranges are used. In the external measurement, the lowest range for the 9-mA signal (5% load) was 500 mA, which is thus a significant uncertainty contributor.

Digital power analyzers are used to perform power measurements. If possible, digital power analyzers and current transducers should be chosen to best meet the requirements for the measurement. However, in most cases, engineers have to rely on their measurement equipment, because alternative configurations are not available. A problem arises when there are no suitable ranges for the external transducers. The large uncertainty

components of measurement devices can lead to significant errors with the input–output measurement method, especially when high-efficiency devices are concerned. Instead, the accuracy of the calorimetric method has been shown to be superior compared with the input–output method. The low uncertainty of efficiency achieved by calorimeters (constant accuracy for losses) makes them suitable as a reference measurement for the input–output method with high-efficiency devices. The results obtained by the calorimetric method are comparable with any switching frequencies, converter topologies, modulation methods, and filter configurations.

VI. Conclusion

This paper presents the results of a European efficiency measurement with input–output and calorimetric methods for a 250-kW high-efficiency grid-connected solar inverter. The electric power was measured by two different sets of equipment. The designed calorimetric system was of an open and balance type. In the loss results, differences were found between the measurement methods. Therefore, an uncertainty analysis was carried out to determine the possible error sources.

References

[1] J. W. Kolar, F. Krismer, Y. Lobsiger, J. Muhlethaler, T. Nussbaumer, and J. Minibock, "Extreme efficiency power electronics," in *Proc. 7th Int. Conf. Integr. Power Electron. Syst.*, Nuremberg, Germany, Mar. 2012, pp. 1–22.

[2] R. Mallwitz and B. Engel, "Solar power inverters," in *Proc. 6th Int. Conf. Integr. Power Electron. Syst.*, Nuremberg, Germany, Mar. 2010, pp. 1–7.

[3] L. Zhang, K. Sun, Y. Xing, L. Feng, and H. Ge, "A modular grid-connected photovoltaic generation system based on DC bus," *IEEE Trans. Power Electron.*, vol. 26, no. 2, pp. 523–531, Feb. 2011.

[4] K. Sun, L. Zhang, Y. Xing, and J. M. Guerrero, "A distributed control strategy based on DC bus signaling for modular photovoltaic generation systems with battery energy storage," *IEEE Trans. Power Electron.*, vol. 26, no. 10, pp. 3032–3045, Oct. 2011.

[5] A. K. Abdelsalam, A. M. Massoud, S. Ahmed, and P. N. Enjeti, "High-performance adaptive perturb and observe MPPT technique for photovoltaic-based microgrids," *IEEE Trans. Power Electron.*, vol. 26, no. 4, pp. 1010–1021, Apr. 2011.

[6] L. Zhou, Y. Chen, K. Guo, and F. Jia, "New approach for MPPT control of photovoltaic system with mutative-scale dual-carrier chaotic search," *IEEE Trans. Power Electron.*, vol. 26, no. 4, pp. 1038–1048, Apr. 2011.

[7] W.-M. Lin, C.-M. Hong, and C.-H. Chen, "Neural-network-based MPPT control of a stand-alone hybrid power generation system," *IEEE Trans. Power Electron.*, vol. 26, no. 12, pp. 3571–3581, Dec. 2011.

[8] S. Khomfoi and C. Aimsaard, "A 5-level cascaded hybrid multilevel inverter for interfacing with renewable energy resources," in *Proc. 6th Int. Conf. Electr. Eng./Electron., Comput., Telecommun. Inf. Technol.*, Bangkok, Thailand, Mar. 2012, pp. 284–287.

[9] P. M. Bhagwat and V. R. Stefanovic, "Generalized structure of a multilevel PWM inverter," *IEEE Trans. Ind. Appl.*, vol. IA-19, no. 6, pp. 1057–1069, Nov./Dec. 1983.

[10] C. J. Hatziadoniu, F. E. Chalkiadakis, and V. K. Feiste, "A power conditioner for a grid-connected photovoltaic generator based on the 3-level inverter," *IEEE Trans. Energy Convers.*, vol. 14, no. 4, pp. 1605–1610, Dec. 1999.

[11] P. K. Hinga, T. Ohnishi, and T. Suzuki, "A new PWM inverter for photovoltaic power generation system," in *Proc. 25th Annu. IEEE Power Electron. Specialists Conf.*, Taipei, Taiwan, Jun. 1994, pp. 1040–1045.

[12] A. Sarwar and M. S. J. Asghar, "Multilevel converter topology for solar PV based grid-tie inverters," in *Proc. IEEE Int. Energy Conf.*, Manama, Bahrain, Dec. 2010, pp. 501–506.

[13] H. J. Kim, Y. H. Chung, K. S. Lee, Y. S. Jon, and K. S. Kim, "Performance analysis of soft-switching inverter for the photovoltaic power system," in *Proc. 7th Int. Conf. Power Electron.*, Daegu, Korea, Oct. 2007, pp. 436–439.

[14] T. C. Y. Wang, Z. Ye, G. Sinha, and X. Yuan, "Output filter design for a grid-interconnected three-phase inverter," in *Proc. IEEE 34th Annu. Power Electron. Spec. Conf.*, Acapulco, Mexico, Jun. 2003, pp. 779–784.

[15] B. Burger, D. Kranzer, and O. Stalter, "Cost reduction of PV-inverters with SiC DMOSFETs," in *Proc. 5th Int. Conf. Integr. Power Electron. Syst.*, Nuremberg, Germany, Mar. 2008, pp. 1–5.

[16] *Overall Efficiency of Grid Connected Photovoltaic Inverters, Ed. 1,* SS-EN 50530, Nov. 2010, pp. 1–36.

[17] H. Haeberlin, L. Borgna, M. Kaempfer, and U. Zwahlen, "Total efficiency ηtot – a new quantity for better characterisation of grid-connected PV inverters," in *Proc. 20th Eur. Photovoltaic Solar Energy Conf.*, Barcelona, Spain, Jun. 2005, pp. 1–4.

[18] *Photovoltaic Systems—Power Conditioners—Procedure for Measuring Efficiency,* IEC 61683, Nov. 1999, pp. 1–20.

[19] V. Mattsson, "Comparison of calorimetric and electrical loss measurement methods in a frequency converter research and development application," in *Proc. IEEE Energy Convers. Cong. Expo.*, Phoenix, AZ, Sep. 2011, pp. 1026–1030.

[20] *Rotating Electrical Machines— Part 2-2: Specific Methods for Determining Separate Losses of Large Machines from Test— Supplement to IEC 60034-2-1, Ed. 1,* IEC 60034-2-2, Mar. 2010.

[21] W. Cao, G. M. Asher, X. Huang, H. Zhang, I. French, J. Zhang, and M. Short, "Calorimeters and techniques used for power loss measurements in electrical machines," *IEEE Instrum. Meas. Mag.*, vol. 13, no. 6, pp. 26–33, Dec. 2010.

[22] B. Baholo, P. H. Mellor, D. Howe, and T. S. Birch, "An automated calorimetric method of loss measurement in electrical machines," *J. Magn. Magn. Mater.*, vol. 133, no. 1–3, pp. 433–436, May 1994.

[23] D. R. Turner, K. J. Binns, B. N. Shamsadeen, and D. F. Warne, "Accurate measurement of induction motor losses using balance calorimeter," *IEE Electr. Power Appl.*, vol. 138, no. 5, pp. 233–242, Sep. 1991.

[24] A. P. Van den Bossche, D. M. Van de Sype, and V. Valchev, "Flow calorimeter for equipment test," in *Proc. IEEE 31st Annu. Conf. Ind. Electron. Soc.*, Raleigh, NC, Nov. 2005, pp. 860–864.

[25] A. Jalilian, V. J. Gosbell, B. S. P. Perera, and P. Cooper, "Double chamber calorimeter (DCC): A new approach to measure induction motor harmonic losses," *IEEE Trans. Energy Convers.*, vol. 14, no. 3, pp. 680–685, Sep. 1999.

[26] K. J. Bradley, W. Cao, and J. Arellano-Padilla, "Evaluation of stray load loss in induction motors with a comparison of input-output and calorimetric methods," *IEEE Trans. Energy Convers.*, vol. 21, no. 3, pp. 682–689, Sep. 2006.

[27] W. Cao, K. J. Bradley, J. C. Clare, and P. W. Wheeler, "Comparison of stray load and inverter-induced harmonic losses in induction motors using calorimetric and harmonic injection methods," *IEEE Trans. Ind. Appl.*, vol. 46, no. 1, pp. 249–255, Jan./Feb. 2010.

[28] W. Cao, K. J. Bradley, and A. Ferrah, "Development of a high-precision calorimeter for measuring power loss in electrical machines," *IEEE Trans. Instrum. Meas.*, vol. 58, no. 3, pp. 570–577, Mar. 2009.

[29] W. Cao, X. Huang, and I. French, "Design of a 300-kW calorimeter for electrical motor loss measurement," *IEEE Trans. Instrum. Meas.*, vol. 58, no. 7, pp. 2365–2367, Jul. 2009.

[30] A. Kosonen, L. Aarniovuori, J. Pyrhönen, M. Niemelä, and J. Backman, "Calorimetric concept for measurement of power losses up to 2 kW in electric drives (accepted for publication)," *IET Electr. Power Appl.*, to be published.

[31] L. Aarniovuori, A. Kosonen, M. Niemelä, and J. Pyrhönen, "Calorimetric measurement of variable-speed induction motor," in *Proc. 20th Int. Conf. Electr. Mach.*, Marseille, France, Sep. 2012, pp. 870–876.

[32] *Evaluation of Measurement Data – Guide to the Expression of Uncertainty in Measurement, Ed. 1,* JCGM 100:2008, Sep. 2008, pp. 1–134.

[33] C. Xiao, G. Chen, and W. G. H. Odendaal, "Overview of power loss measurement techniques in power electronics systems," *IEEE Trans. Ind. Appl.*, vol. 43, no. 3, pp. 657–664, May/Jun. 2007.

Lassi Aarniovuori was born in Jyväskylä, Finland, in 1979. He received the M.Sc. and D.Sc. degrees in electrical engineering from the Lappeenranta University of Technology (LUT), Lappeenranta, in Finland, in 2005 and 2010, respectively.

He is currently a Researcher in the Department of Electrical Engineering, LUT. His current research interests include the field of electric drives, especially simulation of electric drives, efficiency measurements, and calorimetric measurement systems.

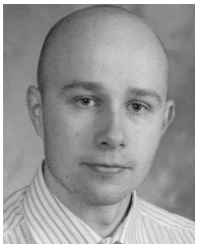

Antti Kosonen was born in Imatra, Finland, in 1980. He received the M.Sc. and D.Sc. degrees in electrical engineering from the Lappeenranta University of Technology (LUT), Lappeenranta, Finland, in 2005 and 2008, respectively.

He is currently researching efficiency measurement methods including calorimeters at the Department of Electrical Engineering, LUT. His current research interests include power line communication, calorimeters, and efficiency measurements.

Pekka Sillanpää was born in Parkano, Finland in 1981. He received the B.Sc. degree in the Department of Electrical Energy, Tampere University of Technology, Tampere, Finland in 2011, where he is currently working toward the M.Sc. degree.

His current research interests in the field of power electronics include efficiency of electric drives and calorimetric and electrical measurement systems.

Markku Niemelä was born in Mäntyharju, Finland, in 1968. He received the B.Sc. degree in electrical engineering from the Helsinki Institute of Technology in 1990, and the M.Sc. and D.Sc. (technology) degrees from the Lappeenranta University of Technology (LUT), Lappeenranta, Finland, in 1995 and 1999, respectively.

He is currently a Senior Researcher with the Carelian Drives and Motor Centre in LUT. His current research interests include motion control, control of line converters, and energy efficiency of electric drives.